Journal of Electrotechnology, Electrical Engineering and Management (2025)
Clausius Scientific Press, Canada
DOI: 10.23977/jeeem.2025.080109
ISSN 2560-6697 Vol. 8 Num. 1

Analysis of Flow Field Characteristics in Proton Exchange Membrane Fuel Cells Based on Bio-Inspired Leaf-Vein Structures

Zhang Anzhuang[1,a], Zhang Tong[1,2,b,*]

[1]*School of Automotive Studies, Tongji University, Shanghai, China*
[2] *Yangtze Delta Region Institute of Tsinghua University, Zhejiang, Jiaxing, 314006, China*
[a]*2231625@tongji.edu.cn,* [b]*tzhang@tongji.edu.cn*
[*]*Corresponding author*

Keywords: Proton exchange membrane fuel cell, Leaf-Vein-Inspired Flow Field, Secondary Flow Channel, Current Density

Abstract: Traditional fuel cell flow field structures often suffer from non-uniform current and reactant distributions, which hinders reaction efficiency and fuel utilization. To address these issues, this study establishes a bio-inspired leaf-vein PEMFC simulation platform based on FLUENT, investigating the impact of various flow field geometries on species distribution, pressure drop, and electrochemical performance. Results show that when the primary–secondary vein angle is set to 30°, the average oxygen concentration at the catalyst layer interface reaches 3.05 mol/m^3, and the current density is well balanced with an average value of 0.70 A/cm^2. Meanwhile, the water saturation at the interface is reduced to 0.13 or below. At 0.4 V, the peak current density reaches 0.97 A/cm^2 with a water removal efficiency exceeding 94%. Introducing secondary branches leads to a 6.3% increase in average reactant concentration at the GDL–CL interface and approximately 20% reduction in pressure drop. Moreover, the high-current-density region shifts about 20% toward the outlet, indicating a better distribution of mass transfer pathways. Overall, under the condition of over 94% water removal efficiency, the parasitic power loss is reduced by approximately 8%.

1. Introduction

Proton exchange membrane fuel cells (PEMFCs), as a representative clean energy technology, have become core power devices in aerospace propulsion systems, new energy vehicles, and distributed generation due to their exceptional energy density, low-temperature startup capability, and rapid response characteristics[1-4].In recent years, with increasing demands for flow uniformity and mass transport efficiency, researchers have sought inspiration from nature to develop flow fields with biomimetic characteristics. Natural systems—such as plant leaf venation and mammalian alveolar structures—have evolved to optimize flow resistance and distribution uniformity. These topological features provide valuable references for the structural design of PEMFC flow channels. Kloess et al.[5] designed flow fields inspired by leaf and lung geometries, which demonstrated lower pressure drops and more uniform gas distribution compared to conventional serpentine and interdigitated designs. Chen et al.[6], using a maize leaf venation pattern as a basis, reported notable performance improvements under low-voltage conditions, along with enhanced gas transport, better water management, and reduced pressure drop. Furthermore, Zhang et al.[7] compared a range of biomimetic geometries—including leaf-like, lung-like, and tree-like structures—and found that all these topologies improved gas distribution uniformity, fuel utilization efficiency, and drainage performance. These improvements led to reduced pressure losses and increased power density. Srinivasa et al.[8] reported that in leaf-vein-inspired flow channels, staggered channel configurations can further enhance net power output. Beyond macroscopic geometry, the cross-sectional shape of the channels also plays a critical role in performance. These findings further confirm that altering the cross-sectional geometry from trapezoidal to triangular can effectively improve oxygen concentration and current density. Leaf-vein-inspired flow fields exhibit excellent performance in improving gas transport and water management. They not only overcome the drainage limitations of parallel flow fields but also reduce pressure losses and parasitic power consumption, thereby improving the overall system efficiency. Based on the insights from previous studies, this work proposes a multi-dimensional optimization strategy. First, the optimal main–branch angle is determined to identify the best geometric configuration. Then, microstructural refinements are introduced to mitigate water accumulation at the channel outlets, ultimately aiming to enhance current density and power output.

2. Establishment of the Simulation Platform

2.1 Development of the Fuel Cell Model

To establish a foundation for the subsequent simulation of leaf-vein-inspired flow fields, a single serpentine flow field model was constructed using ANSYS Fluent for simulation validation, as illustrated in Fig. 1. The computational domain includes the bipolar plates (hidden in the figure), anode and cathode flow channels, gas diffusion layers (GDL), catalyst layers (CL), and the proton exchange membrane (MEM). The simulation was conducted under an operating temperature of 70 °C and a pressure of 1 atm. The anode and cathode stoichiometric ratios were set to 1.5 and 2, respectively, with a relative humidity of 100%. Detailed simulation parameters are provided in Table 1.

Table 1 Geometric and Physical Parameters of the Simulation Model

Parameter	Value
Flow channel width/depth (mm)	1 / 1
Bipolar plate length/width/height (mm)	43 / 11 / 1.5
GDL thickness (mm)	0.3
Catalyst layer (CL) thickness (mm)	0.0129
Membrane thickness (mm)	0.108
porosity of GDL/CL/MEM	0.6/0.3/0.25
Open circuit voltage (V)	$E^0 = 0.0025T + 0.2329$
Operating temperature (K)	343.14
Operating pressure (Pa)	101325
Inlet relative humidity (%)	100
Anode/Cathode stoichiometric ratio	1.5/2
Reference exchange current density (anode) ($A \cdot m^{-3}$)	$j_{a,\mathrm{ref}} = 10^9 \cdot e^{-1400\left(\frac{1}{T}-\frac{1}{353.15}\right)}$
Reference exchange current density (cathode) ($A \cdot m^{-3}$)	$j_{c,\mathrm{ref}} = 10^4 \cdot e^{-7900\left(\frac{1}{T}-\frac{1}{353.15}\right)}$
Reference concentration (anode/ cathode) ($mol \cdot m^{-3}$)	40/4
Concentration exponent (anode)	0.5
Concentration exponent (cathode)	1
Charge transfer coefficient (anode)	1
Charge transfer coefficient (cathode)	1
Air permeability of GDL (m^2)	1.76E-11
Air permeability of catalyst layer (m^2)	1e-12
Specific surface area (m^2/m^3)	200000

2.2 Governing Equations

The operation of a PEMFC involves multiple coupled physical phenomena, including convective and diffusive transport, species variation, and electrochemical reactions. These processes require a comprehensive set of mathematical models to accurately describe the fuel cell's working state. The physical mechanisms occurring within a PEMFC are generally governed by the conservation laws of mass, momentum, energy, species, and charge transport. Accordingly, the mathematical modeling of the PEMFC in this study is based on the following assumptions: The reactant gases (gas mixtures) behave as incompressible ideal gases. Gas flow is assumed to be laminar. The proton exchange membrane and catalyst layers are considered homogeneous and isotropic. Electrical resistance within the solid components of the PEMFC is neglected.

The mass conservation equation is given by:

$$\frac{\partial(\varepsilon\rho)}{\partial t} + \nabla(\varepsilon\rho v) = S_m \tag{1}$$

where ρ is the density of the gas mixture ($kg \cdot m^{-3}$), ε is the porosity of the porous medium. In the anode gas flow channel, ε typically takes a value of 1, while in porous electrodes and catalyst layers, it satisfies $\varepsilon<1$. $\boldsymbol{u}$ is the fluid velocity vector. S_m represents the mass source term.

Mass Source Term in the Anode:

$$S_{ma} = -\frac{M_{H_2} R_a}{F} \tag{2}$$

Mass Source Term in the Cathode:

$$S_{mc} = -\frac{M_{O_2} R_c}{4F} - \frac{M_{H_2O} R_c}{F} \tag{3}$$

where M denotes the molar mass of the respective species, F is the Faraday constant, and R represents the exchange current density ($A \cdot m^{-3}$) corresponding to the reaction per unit volume in the anode or cathode.

Momentum Conservation Equation:

$$\frac{\partial(\varepsilon\rho v)}{\partial t} + \nabla(\varepsilon\rho v v) = -\varepsilon\nabla p + \nabla(\varepsilon\mu\nabla \mathbf{v}) + S_{\mathbf{v}} \tag{4}$$

where p is the gas-phase pressure (Pa), μ is the dynamic viscosity of the gas mixture, and $S_{\mathbf{v}}$ is the momentum source term.

The energy conservation equation is expressed as:

$$\frac{\partial\left(\varepsilon\rho c_p T\right)}{\partial t} + \nabla\cdot\left(\varepsilon\rho c_p vT\right) = \nabla\cdot(k_{eff}\nabla T) + S_Q \tag{5}$$

where c_p is the average specific heat capacity of the gas mixture ($J\cdot(kg\cdot K)^{-1}$), T is the temperature (K), k_{eff} is the effective thermal conductivity ($W\cdot(m\cdot K)^{-1}$), and S_Q is the energy source term ($W\cdot m^{-3}$).

Total Energy Source Term S_Q:

$$S_Q = i_s^2 R_{ohm} + \beta\, i_s\eta + S_{H_2O}^{g} h_{lg} + R_w h_{rea} \tag{6}$$

Where i_s is the effective current density, R_{ohm} is the ohmic resistance per unit volume, β is the electrochemical reaction enthalpy efficiency factor, inη is the net reaction current density, η is the overpotential, $S_{H_2O}^{g}$ is the source term for generated water vapor, h_{lg} is the latent heat of vaporization, R_w is the phase change rate of liquid water, h_{rea} is the enthalpy change of reaction.

The Species Conservation Equation is given by:

$$\frac{\partial(\varepsilon c_k)}{\partial \mathrm{t}} + \nabla \cdot (\varepsilon \boldsymbol{v}\, c_k) = \nabla \cdot \left(D_k^{\mathrm{eff}} \nabla c_k\right) + S_k \tag{7}$$

Where c_k is the concentration of species k, D_k^{eff} is the effective diffusion coefficient of species k, S_k is the source term of species k.

Species Source Terms Based on Faraday's Law:

$$\begin{cases} S_{H_2} = -\dfrac{1}{2F} R_a \\ S_{O_2} = -\dfrac{1}{4F} R_c \\ S_{H_2O} = \dfrac{1}{2F} R_c \end{cases} \tag{8}$$

Where R_a is the volumetric reaction rate in the anode, R_c is the volumetric reaction rate in the cathode, F is the Faraday constant.

The Charge Conservation Equations is given by:

According to the principle of charge conservation, electron and proton currents are transported through different pathways within the fuel cell. The corresponding governing equations are as follows:

Solid Phase (Electron) Current Conservation:

$$\nabla \cdot (\sigma_s \nabla \phi_s) + S_{\phi_s} = 0 \tag{9}$$

Membrane Phase (Proton) Current Conservation:

$$\nabla \cdot (\sigma_m \nabla \phi_m) + S_{\phi_m} = 0 \tag{10}$$

Where σ_s and σ_m are the electrical conductivities of the solid and membrane phases, respectively ($\mathrm{S \cdot m^{-1}}$), ϕ_s and ϕ_m represent the electric potentials in the solid and membrane phases (V), S_{ϕ_s} and S_{ϕ_m} are the source terms for the solid-phase and membrane-phase potentials, respectively, arising from electrochemical reactions.

Butler–Volmer Equation:

The electrochemical reaction source terms at the anode and cathode are expressed using the Butler–Volmer equations as follows:

$$S_a = \zeta j_{\mathrm{ref}} \left(\frac{C_{H_2}}{C_{H_2,\mathrm{ref}}}\right)^{\gamma_a} \left[e^{\frac{\alpha_a F \eta_a}{RT}} - e^{-\frac{\alpha_c F \eta_a}{RT}}\right] \tag{11}$$

$$S_c = \zeta j_{\mathrm{ref}} \left(\frac{C_{O_2}}{C_{O_2,\mathrm{ref}}}\right)^{\gamma_c} \left[e^{\frac{\alpha_c F \eta_c}{RT}} - e^{-\frac{\alpha_a F \eta_c}{RT}}\right] \tag{12}$$

Where S_a and S_c denote the electrochemical source terms at the anode and cathode, respectively, j_{ref} is the reference exchange current density ($\mathrm{A \cdot m^{-3}}$),ζ is the active surface area per unit volume ($\mathrm{m^2 \cdot m^{-3}}$), C and C_{ref} are the local and reference molar concentrations of the reactants ($\mathrm{mol \cdot m^{-3}}$), γ is the reaction order, T is the operating temperature (K), α_a and α_c are the anodic and cathodic transfer coefficients, respectively, η is the activation overpotential (V), V_{oc} is open circuit voltage

2.3 Model Validation

In this simulation study, mesh independence verification and model validation were carried out based on different mesh resolutions. This approach not only improves the accuracy of data during the computational process but also significantly reduces computational time and cost. Meshes with varying resolutions were tested, with element sizes set to 200 µm, 250 µm, and 320 µm. The corresponding mesh element counts were approximately 2 million, 3 million, and 6 million, respectively. As shown in Figure 1, after comparing the simulation outcomes at mesh sizes of 200 µm, 250 µm, and 320 µm, the final mesh size of 250 µm was selected for subsequent calculations.

Under operating conditions of 70 °C cell temperature, 1 atm outlet gas pressure, 100% relative humidity at the cathode, and an anode-to-cathode flow rate ratio of 1:1.2, model validation was conducted. Current density measurements were recorded starting from a cell voltage of 0.9 V, with a step size of 0.05 V, and ending at 0.4 V. The simulation results (as shown in Figure 2) from this model showed good agreement with the experimental data, indicating that the model predictions are reliable. Based on this validated model, further studies were carried out to investigate the bio-inspired leaf-vein flow field.

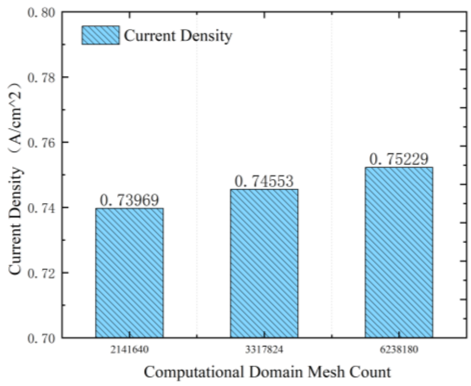

Figure 1 Mesh Independence Verification

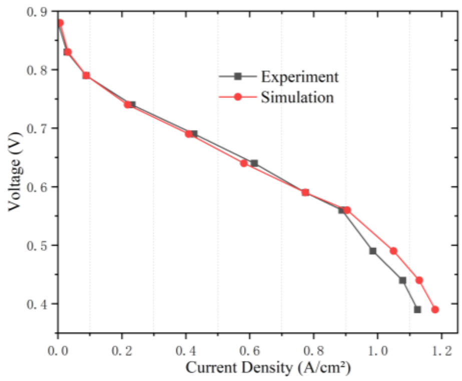

Figure 2 Polarization Curve: Simulation and Experimental Validation

2.4 Research Design

In this chapter, eight leaf-vein-inspired flow field configurations were designed to compare the electrochemical performance and species distribution under various experimental conditions. The included configurations feature bifurcation angles from 15 ° to 35 ° at 5 ° intervals. On this basis, secondary channels were introduced, and at 45 °, further structural modification was conducted by offsetting the branch node positions. These models(D2) were used to compare species distribution and electrochemical performance under identical working conditions.

Each flow field model has an average cross-sectional area of 32 mm × 32 mm, with a uniform channel width and depth of approximately 1 mm. Figure 3 shows representative flow field geometries with different bifurcation angles (example shown for α = 45°). The secondary flow channels were introduced at a 30 °angle relative to the primary–secondary branch channels, with a width of 0.8 mm and a depth of 1 mm. These channels were interconnected at each level and arranged parallel to the main channels. Figure 3 presents the structural diagram of the leaf-vein-inspired flow field with secondary branches. To further investigate the influence of branch positioning on flow performance, three variations of node offset were developed under the 45 °condition: no offset, 1/2 offset, and 1/3 offset. The performance impact of each configuration was analyzed accordingly.

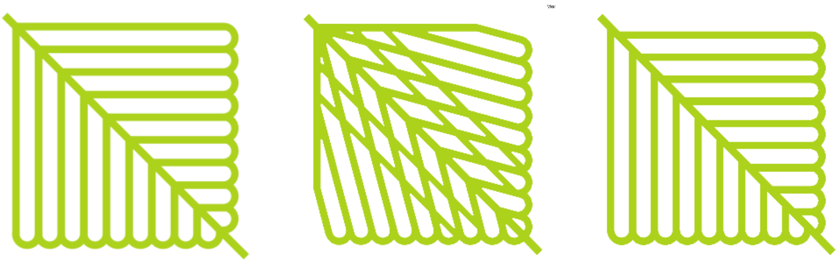

45 °　　secondary channels　　D2

Figure 3 Schematic Diagram of the Flow Field Structure

3. Results and Discussion

3.1 Effect of Flow Field Structure on Oxygen Distribution

To assess the impact of flow field geometry on oxygen distribution in PEMFCs, oxygen concentration profiles were evaluated for eight leaf-vein-inspired designs under 0.7 V.

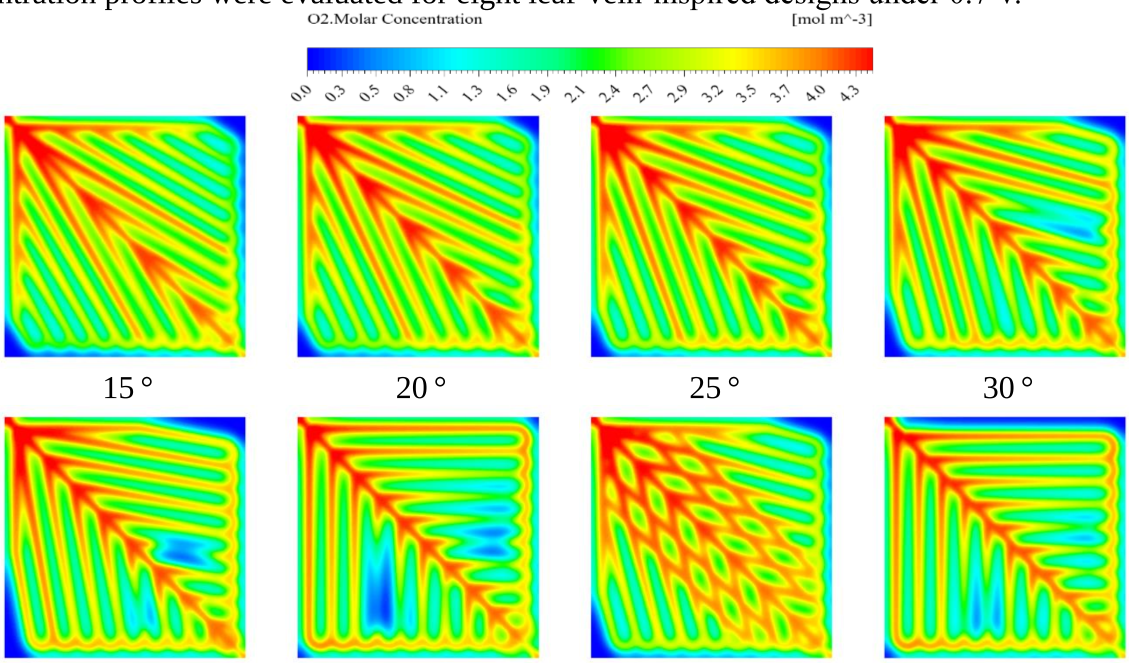

Figure 4 Oxygen Molar Concentration Distribution

Varying the main–branch bifurcation angle from 15 ° to 45 ° revealed a clear gradient from high inlet to low outlet concentration (as shown in Figure 4). As the angle increased from 15 ° to 25 °, the average oxygen concentration (as shown in Figure 5) rose from 2.667 to 2.754 mol/m^3, enhancing reactant balance. However, at 45°, the average dropped to 2.537 mol/m^3, with severe outlet "dead zones." The 25°–30 ° range was identified as optimal and served as a baseline for further refinement. Introducing secondary transverse branches at 30 ° improved lateral diffusion, increasing the average concentration from 2.701 to 2.870 mol/m^3 (+6.3%) and reducing outlet deficits. This agrees with Fick's law, where the enhanced transverse pathways smooth gradients and alleviate local starvation. Additionally, implementing a 1/3 node offset at 45 ° (D2 scheme) yielded a more uniform distribution, lowering the outlet concentration difference to 1.35×10^2 mol/m^3 and mitigating downstream flow maldistribution. Overall, the optimal strategy combines a 25 °–30 ° bifurcation angle, secondary branching, and fine node adjustment to boost average oxygen availability and suppress starvation, achieving coordinated enhancement of transport and uniformity in PEMFC cathodes.

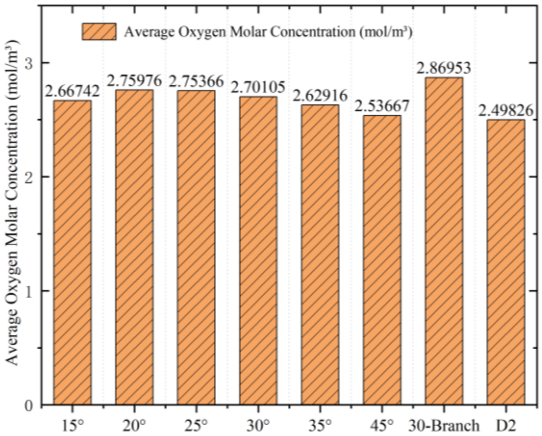

Figure 5 Average Oxygen Molar Concentration

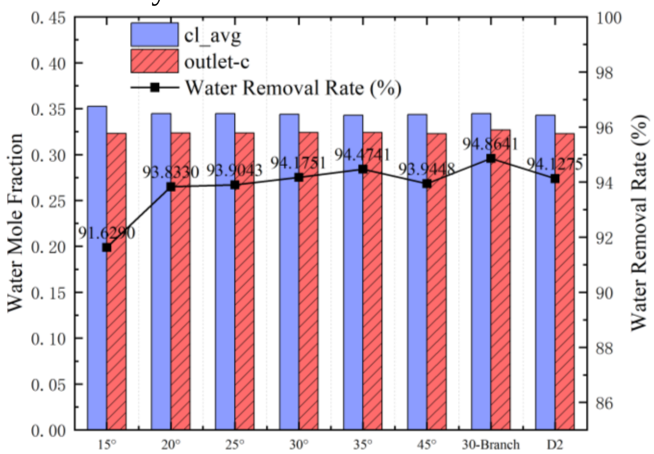

Figure 6 Water Mole Fraction Distribution

3.2 Effect of Flow Field Structure on Cathode Water Distribution

To investigate this issue, we analyzed three structural categories of leaf-vein-inspired flow fields: variation of the main–branch bifurcation angle (15°–45°); addition of secondary branch channels at a 30° baseline; and branch node offset (1/3 offset, D2 scheme) based on the 45° structure. We conducted a systematic evaluation of water mole fraction distribution and water removal efficiency at the CL–GDL interface.

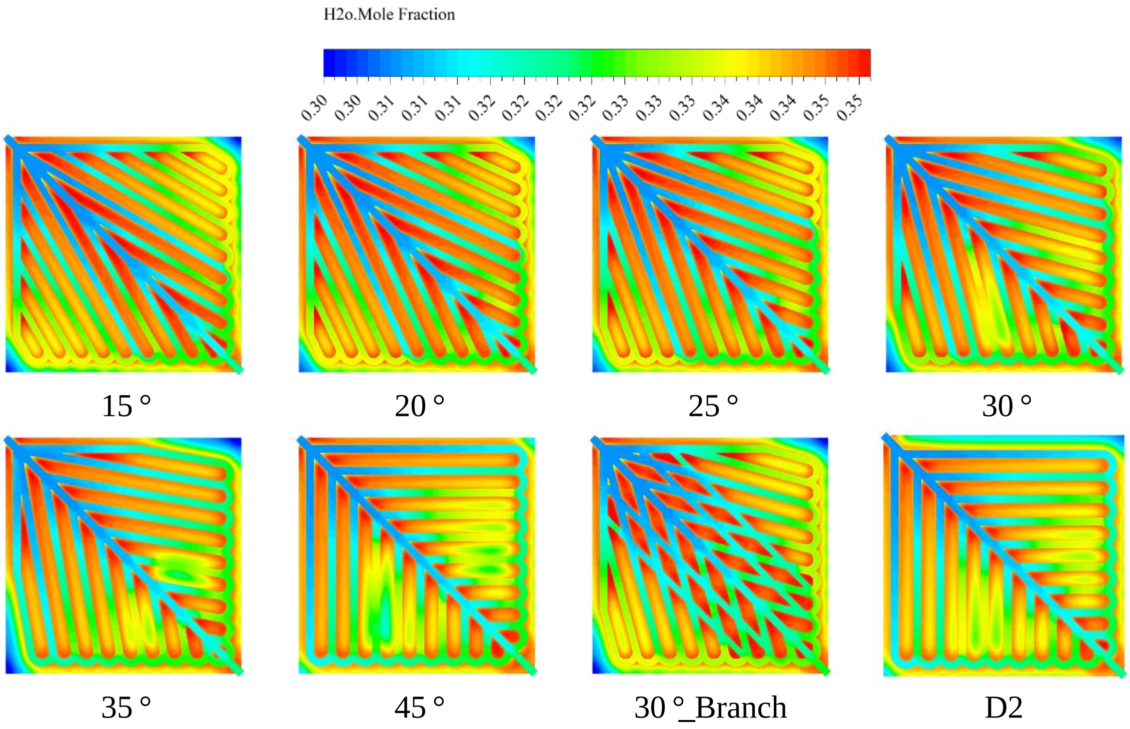

Figure 7 Contour Plot of Water Mole Fraction Distribution

Firstly, in the main–branch angle variation group, as the angle increased from 15° to 35°, the average water mole fraction at the CL–GDL interface (as shown in Figure 6) decreased from 0.3526 to 0.3430 (a 2.72% reduction), while water removal efficiency increased from 91.63% to 94.47%. When the angle (as shown in Figure 7) further increased to 45°, the water mole fraction rose slightly to 0.3435 (+0.15%), and the water removal efficiency dropped to 93.94%, indicating that the 25°–35° range achieves the best balance between water retention and drainage. Next, for the case with additional secondary branches, the average water mole fraction improved from 0.3439 to 0.34456, and the outlet water mole fraction increased from 0.32395 to 0.32687. Water removal efficiency rose from 94.18% to 94.86%, confirming that transverse sub-channels effectively enhance drainage and mitigate outlet flooding. Finally, in the D2 node-offset configuration based on the 45° flow field, the average water mole fraction decreased further to 0.3355, and the outlet water mole fraction dropped to 0.3202. Water removal efficiency improved from 93.25% to 94.00%. These results show that appropriate micro-adjustment of the node position can reduce uneven flooding in local regions, thus enhancing terminal drainage and improving overall water management.

In summary, the optimal performance is achieved by selecting a bifurcation angle of 25°–35°, followed by the introduction of secondary sub-channels, and finally applying precise node-offset strategies. This multiscale hierarchical optimization ensures adequate water removal without compromising humidification, ultimately achieving refined control over water transport and retention in PEMFCs.

3.3 Effect of Flow Field Structure on Pressure Drop in PEMFC

At an operating voltage of 0.7 V, the pressure drop in the cathode side of each bio-inspired flow field configuration exhibited clear structural dependence. First, in the group of pure primary–secondary branch structures, as the bifurcation angle increased from 15° to 35°, the pressure drop fluctuated slightly within a narrow range of 214–223 Pa, peaking at 223.5 Pa for 25°, and reaching a minimum of 214.8 Pa at 15°. This indicates that mild geometric variation in this range produces relatively stable flow resistance. However, at 45°, the pressure drop spiked to 348.9 Pa, primarily due to the overly dense network of branching channels, which significantly shortened the effective flow length and increased the frequency of local flow turning and shearing, thereby drastically increasing viscous losses. In contrast, adding transverse secondary branches to the 30° configuration ("30-Branch") resulted in a significant reduction in pressure drop to 176.9 Pa—the lowest among all tested cases. This demonstrates that the presence of transverse fine channels not only promotes uniform gas distribution but also helps redistribute volumetric flow, reducing velocity gradients and local turbulence. When the 45° structure was modified with a 1/3 node offset ("D2" configuration), the pressure drop was reduced to 270.2 Pa. Although this is still higher than in the 30-Branch case, it significantly improved upon the unmodified 45° case. The offset geometry mitigated the extreme congestion and pressure rise caused by abrupt local turning in the terminal branches.

In conclusion, choosing a bifurcation angle between 25° and 35° ensures low and stable pressure drop. The addition of secondary branches helps reduce flow resistance and improves flow uniformity, while node offset serves as a fine-tuning method to control pressure losses in high-angle configurations. These findings offer valuable insights for the low-resistance design of PEMFC flow fields, aiding in the coordinated optimization of oxygen transport and overall gas management performance.

3.4 Effect of Flow Field Structure on Electrochemical Performance in PEMFC

Figure 8 shows the current density distributions under 0.7 V for different main–branch bifurcation angles and configurations. Combining this with the pressure drop distribution (as shown in Figure 9), a more detailed analysis can be performed.

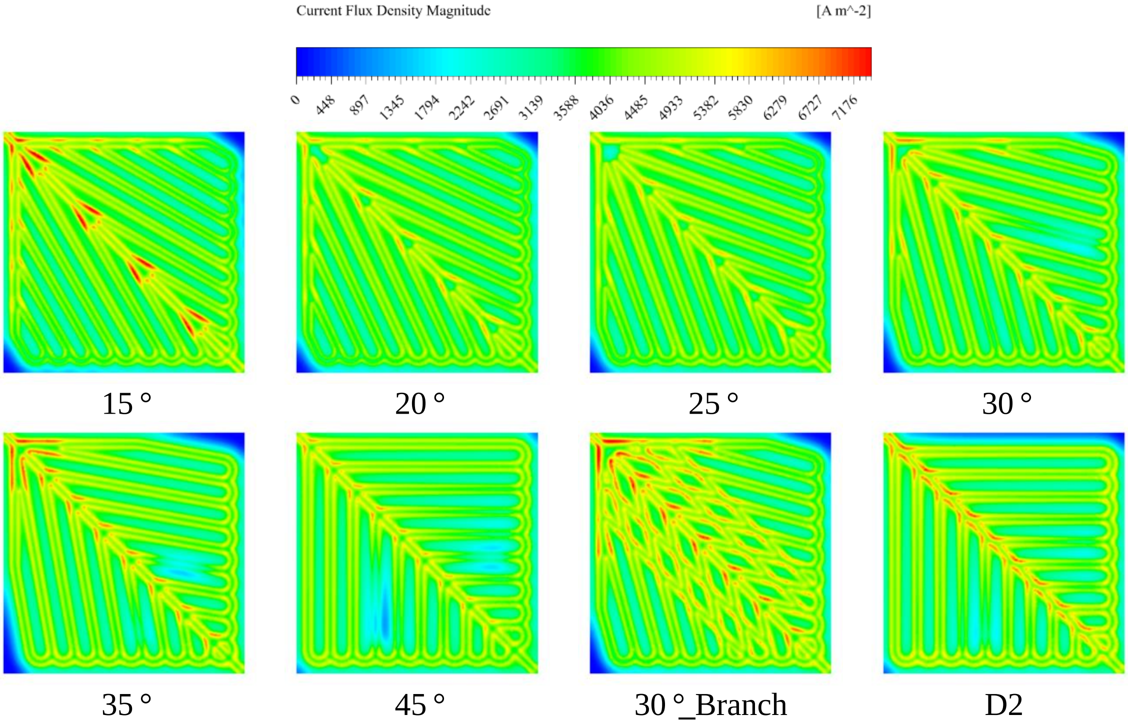

Figure 8 Contour Plot of Current Density Distribution

The polarization curves are shown in Figure 10. In this study, ANSYS Fluent was used to simulate and compare the electrochemical performance of various leaf-vein-inspired flow fields at the cathode catalyst layer. The initial analysis focused on pure main–branch structures with bifurcation angles of 15 ° to 45 °. At lower angles (15 °–20 °), current density was concentrated near the inlet and upper branches, while downstream regions showed significant underutilization, with values around 0.83–0.85 A/cm² at 0.4 V. As the angle increased to 25 °–35 °, high current density regions expanded toward the outlet, and the peak current density rose to 0.88–0.90 A/cm². The corresponding polarization curves shifted upward, indicating improved water transport and enhanced reaction kinetics.

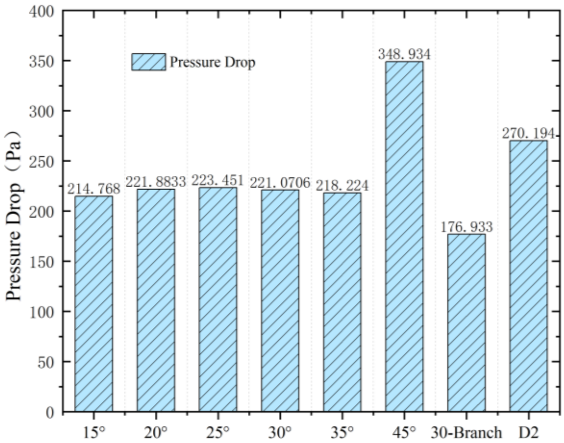

Figure 9 Pressure Drop

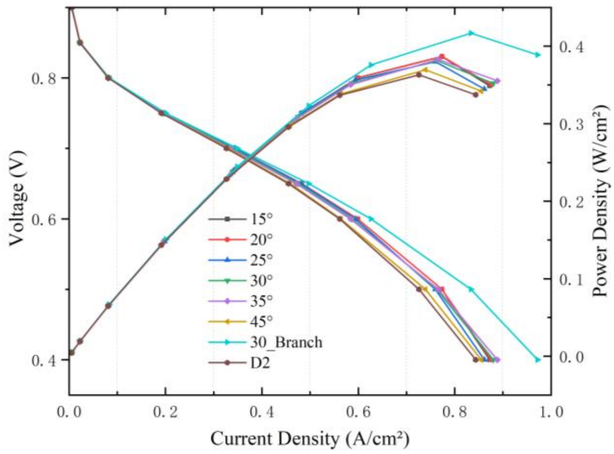

Figure 10 Current Density

When the bifurcation angle increased to 45 °, local inlet utilization improved, but downstream activity declined. Peak current density dropped from ~0.90 to ~0.85 A/cm², and polarization performance worsened due to restricted gas supply and drainage, as well as elevated local resistance from dense branching. To resolve this, a secondary branch structure was added to the optimal 30° configuration. This expanded the high-current-density zone to over one-third of the domain at both 0.4 V and 0.6 V. Average current density improved from 0.880 to 0.972 A/cm² (+10.4%) at 0.4 V, and from 0.587 to 0.626 A/cm² (+6.6%) at 0.6 V, with increased peak power density—attributed to improved oxygen redistribution, reduced flooding, and enhanced lateral diffusion.

Additionally, applying a 1/3 node offset to the 45° baseline (D2 scheme) improved downstream performance. Although peak current density at the inlet slightly declined, the red zone became more continuous downstream, with 10% better surface uniformity. Power density at 0.4 V and 0.6 V increased by ~2–3%, indicating reduced starvation and better reactant utilization.

In summary, the combined strategy of optimizing the bifurcation angle (25°–35°), adding secondary branches, and applying node offsets significantly improves current uniformity and power output. This hierarchical refinement enhances gas and water transport, balances local gradients, and provides a robust design pathway for high-performance PEMFC flow fields.

4. Conclusions

In this study, a series of bio-inspired cathode flow field models for PEMFCs were developed using ANSYS Fluent. Three structural strategies were examined: adjusting the main–branch bifurcation angle (15°–45°), adding secondary transverse branches to the 30° baseline (30-Branch), and applying a 1/3 node offset to the 45° structure (D2). Increasing the angle from 15° to 30° improved oxygen distribution (2.667 → 2.754 mol/m³), reduced water saturation (0.3526 → 0.3430), maintained low pressure drop (214–223 Pa), and expanded the high-current-density zone downstream (peak >0.88 A/cm² at 0.4 V). However, at 45°, oxygen concentration dropped (2.537 mol/m³), pressure rose (349 Pa), and flooding worsened, reducing performance. Introducing secondary branches enhanced lateral transport, raised oxygen concentration to 2.870 mol/m³ (+6.3%), improved water removal (94.86%), and lowered pressure drop to 176.9 Pa (−19.9%). Current density also increased by 10.4% and 6.6% at 0.4 V and 0.6 V. Node offset at 45° further stabilized gas–liquid distribution, with oxygen at ~2.50 mol/m³, pressure reduced to 270 Pa, and removal efficiency rising to 94.20%. In summary, combining a 25°–30° bifurcation angle, secondary branching, and node offset offers an effective multiscale strategy to enhance PEMFC flow field performance, delivering improved transport uniformity, lower losses, and greater long-term efficiency.

References

[1] ZHU D, AIT-AMIRAT Y, N'DIAYE A, et al. Active thermal management between proton exchange membrane fuel cell and metal hydride hydrogen storage tank considering long-term operation [J]. Energy Conv Manag, 2019, 202.

[2] WANG Y, SHI Y, LUO Y, et al. Dynamic analysis of a micro CHP system based on flame fuel cells [J]. Energy Conv Manag, 2018, 163: 268-277.

[3] PEI P, LI Y, XU H, et al. A review on water fault diagnosis of PEMFC associated with the pressure drop [J]. Applied Energy, 2016, 173: 366-85.

[4] HU D, WANG Y, LI J, et al. Investigation of optimal operating temperature for the PEMFC and its tracking control for energy saving in vehicle applications [J]. Energy Conv Manag, 2021, 249.

[5] KLOESS J P, WANG X, LIU J, et al. Investigation of bio-inspired flow channel designs for bipolar plates in proton exchange membrane fuel cells [J]. Journal of Power Sources, 2009, 188(1): 132-140.

[6] SUáREZ C, IRANZO A, TOHARIAS B, et al. Experimental and numerical Investigation on the design of a bioinspired PEM fuel cell [J]. Energy, 2022, 257.

[7] ZHANG S, XU H, QU Z, et al. Bio-inspired flow channel designs for proton exchange membrane fuel cells: A review [J]. Journal of Power Sources, 2022, 522.

[8] BADDURI S R, SRINIVASULU G N, RAO S S. Influence of bio-inspired flow channel designs on the performance of a PEM fuel cell [J]. Chinese Journal of Chemical Engineering, 2020, 28(3): 824-831.